

Ferromagnetic polar metals via epitaxial strain: a case study of SrCoO₃

Zhiwei Liu^{1,2,3}, Qiuyue Li^{1,2,3} and Hanghui Chen^{2,3,4,*}

¹*Key Laboratory of Polar Materials and Devices, Ministry of Education,
East China Normal University, Shanghai 200241, China*

²*NYU-ECNU Institute of Physics, NYU Shanghai, Shanghai 200124, China*

³*Department of Electronic Science, East China Normal University, Shanghai 200241, China*

⁴*Department of Physics, New York University, New York 10012, USA*

**Email: hanghui.chen@nyu.edu*

(Dated: July 11, 2024)

Abstract

While polar metals are a metallic analogue of ferroelectrics, magnetic polar metals can be considered as a metallic analogue of multiferroics. There have been a number of attempts to integrate magnetism into a polar metal by synthesizing new materials or heterostructures. Here we use a simple yet widely used approach—epitaxial strain in the search for intrinsic magnetic polar metals. Via first-principles calculations, we study strain engineering of a ferromagnetic metallic oxide SrCoO₃, whose bulk form crystallizes in a cubic structure. We find that under an experimentally feasible biaxial strain on the *ab* plane, collective Co polar displacements are stabilized in SrCoO₃. Specifically, a compressive strain stabilizes Co polar displacements along the *c* axis, while a tensile strain stabilizes Co polar displacements along the diagonal line in the *ab* plane. In both cases, we find an intrinsic ferromagnetic polar metallic state in SrCoO₃. In addition, we also find that a sufficiently large biaxial strain (> 4%) can yield a ferromagnetic-to-antiferromagnetic transition in SrCoO₃. Our work demonstrates that in addition to yielding emergent multiferroics, epitaxial strain is also a viable approach to inducing magnetic polar metallic states in quantum materials.

I. INTRODUCTION

Ferroelectric [1–4] and multiferroic [5–8] materials have wide applications. By definition, they are insulators with a spontaneous polarization below a Curie temperature and the polarization is switchable by an external electric field [9]. Usually, it is difficult to stabilize a macroscopic polarization in metals since itinerant electrons screen internal dipoles and suppress spontaneous polar displacements. In 1965, Anderson and Blount proposed that if the optical phonons that are responsible for the polar displacements have weak couplings to itinerant electrons, a ferroelectric-like structural phase transition may occur even in a metal at finite temperatures [10]. The prediction was confirmed in 2013 when Shi et al. successfully synthesized LiOsO_3 and observed a continuous centrosymmetric-to-polar structural phase transition around 140 K [11]. Since then, the study of polar metals, the metallic analogue of ferroelectrics, has drawn great attention [12–17], not only because of interests in basic sciences [18] but also in potential technological applications such as electrodes in ferroelectric nanocapacitors [19]. More recently, a number of attempts have been made to integrate magnetism into a polar metal [20–24]. A magnetic polar metal is the metallic analogue of multiferroics. Experimentally, magnetic polar metallic states have been found in $\text{Pb}_2\text{CoOsO}_6$ [20], Fe-doped $\text{Ca}_3\text{Ru}_2\text{O}_7$ [21], $\text{BaTiO}_3/\text{SrRuO}_3/\text{BaTiO}_3$ heterostructure [22] and AA' -stacked $(\text{Fe}_{0.5}\text{Co}_{0.5})_5\text{GeTe}_2$ [23, 24]. However, all these materials either have complicated chemical composition or are artificial heterostructures. On the other hand, epitaxial strain has been widely used to tune physical properties of quantum materials [25], in particular polarization [26]. Well-known examples include strain-induced ferroelectricity in SrTiO_3 , EuTiO_3 and SrMnO_3 [27–30], as well as a strain-driven morphotropic phase boundary in BiFeO_3 [31]. Thus, it is worthwhile to study whether strain engineering can also be utilized to induce a magnetic polar metallic state in known materials.

In this work, we demonstrate how to use epitaxial strain to stabilize an intrinsic ferromagnetic polar metallic state in a known complex oxide SrCoO_3 . Bulk SrCoO_3 is a metal and crystallizes in a simple cubic structure [32]. It exhibits ferromagnetic order below $T_c = 305$ K [33]. We use first-principles calculations and find that an experimentally feasible biaxial strain, either compressive or tensile, can break inversion symmetry in metallic SrCoO_3 . Specifically, we find that under a biaxial compressive strain of 2.4% to 4% imposed on the ab plane, collective Co displacements along the c axis are stabilized, while under a biaxial

tensile strain of 2.9% to 4% imposed on the ab plane, collective Co displacements along the diagonal line in the ab plane are stabilized. In both cases, inversion symmetry is broken via a centrosymmetric-to-polar structural transition and an intrinsic ferromagnetic polar metallic state is induced in SrCoO₃. Furthermore, we find that under a sufficiently large biaxial strain ($> 4\%$), a ferromagnetic-to-antiferromagnetic transition may occur to SrCoO₃. Our work shows that in addition to synthesizing new materials or heterostructures, we can also use strain engineering as a viable approach to searching for magnetic polar metals.

II. COMPUTATIONAL DETAILS

We perform density functional theory (DFT) [34, 35] calculations, as implemented in Vienna Ab Initio Simulation Package (VASP) [36, 37]. We use the generalized gradient approximation with the Perdew-Burke-Ernzerhof parameterization (GGA-PBE) [38] as the exchange-correlation functional. An energy cutoff of 600 eV is used throughout the calculations. The Brillouin zone [39] integration is performed with a Gaussian smearing of 0.05 eV over a Monkhorst-Pack \mathbf{k} -mesh of $16 \times 16 \times 16$ for 5-atom simulation cell and a Monkhorst-Pack \mathbf{k} -mesh of $10 \times 10 \times 8$ for $\sqrt{2} \times \sqrt{2} \times 2$ 20-atom supercell. The convergence threshold for the self-consistent calculation is 10^{-8} eV. Atomic relaxation is converged when each force component is smaller than 10^{-3} eV/Å and pressure on the simulation cell is less than 0.5 kbar. We use the finite-displacement method [40, 41] with the aid of Phonopy [42] to calculate phonon band structure and phonon density of states. For biaxial strain calculations, we fix the two in-plane lattice constants (a and b) and allow the out-of-plane lattice constant (c axis) to fully relax. The strain is defined as $\xi = (a - a_{\text{opt}})/a_{\text{opt}} \times 100\%$ where a_{opt} is the DFT optimized lattice constant of ferromagnetic cubic SrCoO₃ and a is the theoretical lattice constant of the substrate that imposes biaxial strain. All the calculations are spin polarized. To consider the correlation effects in SrCoO₃, we test a range of U on Co- d orbitals using the spin polarized DFT+ U method. We find that for both lattice constant and magnetization, $U = 0$ yields the best agreement between theory and experiment. Increasing U , however, impairs the agreement. Therefore we choose $U = 0$ in our calculations. See Supplemental Material [43] Note 1 for details. Since polarity and magnetism both originate from Co atom and the atomic number of Co is small, we neglect spin-orbit interaction in this study. We use the Aflow library (Automatic FLOW for Materials Discovery www.afloplib.org/afloplib-online)

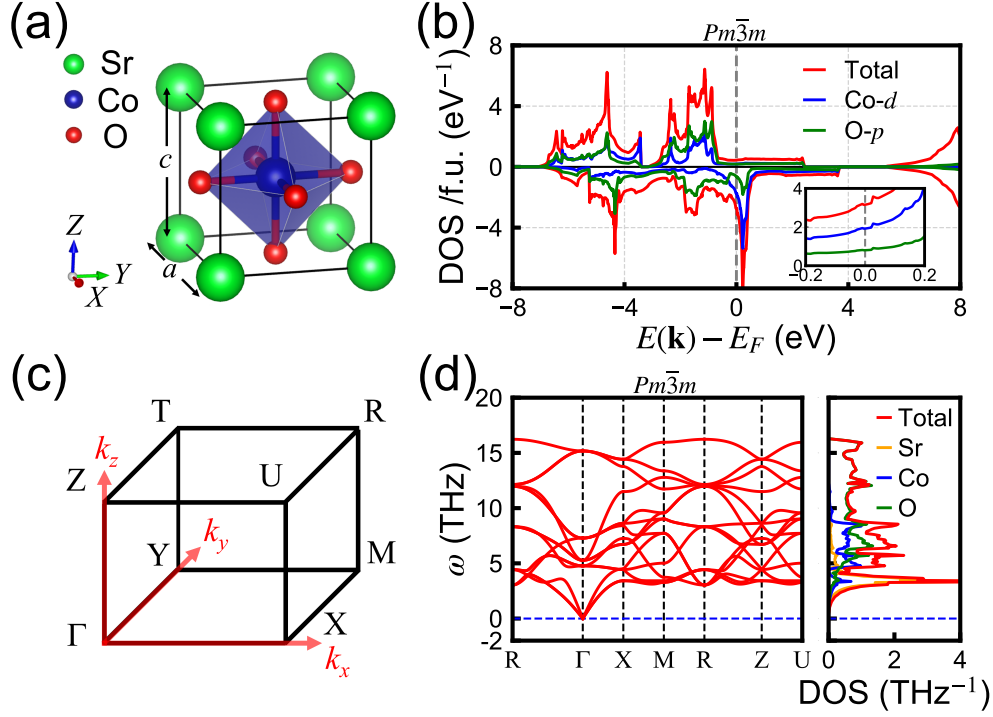


FIG. 1. (a): The crystal structure of cubic SrCoO₃. The green, blue and red balls represent Sr, Co and O atoms, respectively. (b): Density of states (DOS) of cubic SrCoO₃. The red, blue and green curves are total, Co-*d* projected and O-*p* projected DOS. Inset: near-Fermi-level DOS (spin up + spin down) of cubic SrCoO₃. (c): $\frac{1}{8}$ Brillouin zone of cubic SrCoO₃. (d): Phonon band structure and phonon DOS of cubic SrCoO₃. The coordinates of the high-symmetry \mathbf{k} -points are: $R(0.5, 0.5, 0.5)$, $\Gamma(0.0, 0.0, 0.0)$, $X(0.5, 0.0, 0.0)$, $M(0.5, 0.5, 0.0)$, $Z(0.0, 0.0, 0.5)$, $U(0.5, 0.0, 0.5)$. The red, orange, blue and green curves are total, Sr projected, Co projected and O projected phonon DOS.

to determine the space group of various SrCoO₃ crystal structures and also use Phonopy to cross-check it.

III. RESULTS

A. Bulk

First, we calculate bulk properties of SrCoO₃. Experimentally, SrCoO₃ crystalizes in a simple cubic structure without any oxygen octahedral rotations. The corresponding space group is $Pm\bar{3}m$ (no. 221) and the corresponding Glazer notation is $a^0a^0a^0$ [45]. Bulk

SrCoO₃ is a ferromagnetic metal below 305 K with a saturation magnetic moment of 2.5 μ_B /f.u. at 2 K [33]. Fig. 1(a) shows the optimized crystal structure of bulk SrCoO₃ in our DFT calculations. We find that it is stabilized in a cubic structure with the optimized lattice constant $a_{\text{opt}} = 3.827 \text{ \AA}$, which is in good agreement with experiment and the previous theoretical studies [33, 46–49]. Fig. 1(b) shows the density of states (DOS) of bulk SrCoO₃. The DOS clearly shows a ferromagnetic metallic state with the exchange splitting being about 1 eV. Around the Fermi level, there are Co-*d* and O-*p* states, which are strongly hybridized with each other. Fig. 1(c) shows the Brillouin zone of an orthogonal crystal structure (cubic structure is a special case), in which all the high-symmetry \mathbf{k} -points are labelled. They are used in this figure as well as in the subsequent figures. Fig. 1(d) shows the phonon spectrum and density of states of cubic SrCoO₃. We find that cubic SrCoO₃ is free from imaginary phonon modes, indicating that the cubic structure is stable. From the phonon spectrum, we find that the low-frequency phonons are mainly associated with the vibration of Sr atoms since Sr atoms are the heaviest among SrCoO₃, while the high-frequency phonons are associated with the vibration of O atoms because O atoms have light mass. The above results show that DFT provides a reasonable description of electronic and structural properties of bulk SrCoO₃.

B. Compressive strain

Next we study SrCoO₃ under compressive biaxial strain. Under a compressive strain, cubic SrCoO₃ naturally transforms to a tetragonal structure with $c/a > 1$. However, the simple tetragonal structure with no other distortions is not necessarily dynamically stable. To carefully check this point, we perform phonon calculations on the simple tetragonal structure of SrCoO₃ under various compressive strains. We show the results in Fig. 2. We find that under 1% and 2% compressive strains, SrCoO₃ is stabilized in a simple tetragonal structure with no other distortions. This corresponds to space group $P4/mmm$ (no. 123) and Glazer notation ($a^0a^0c^0$). However, under 3% and 4% compressive strains, imaginary phonon modes appear at Γ , M , R and X points, indicating that other structural distortions may occur in the simple tetragonal structure [50]. By analyzing the vibration modes, we find that the imaginary phonon at Γ point is a polar mode with the Co and O atoms moving out-of-phase along the c -axis; the imaginary phonon at M point is a mode in which the

CoO₆ oxygen octahedra rotate in-phase about the c -axis; the imaginary phonon at R point is a mode in which the CoO₆ oxygen octahedra rotate out-of-phase about the c -axis; the imaginary phonon at X point is an anti-polar mode with Co and O atoms forming an “out-of-phase local polarization” that alternates its direction unit cell by unit cell along a axis. We note that due to the C_4 rotation symmetry of the simple tetragonal structure, Y point is equivalent to X point in the Brillouin zone and there is another imaginary anti-polar mode at Y point with Co and O atoms forming an “out-of-phase local polarization” that alternates its direction unit cell by unit cell along b axis. Introducing those phonon modes into the simple tetragonal structure will lower the total energy and yield a new crystal structure, in which a ferromagnetic polar metallic state may be stabilized.

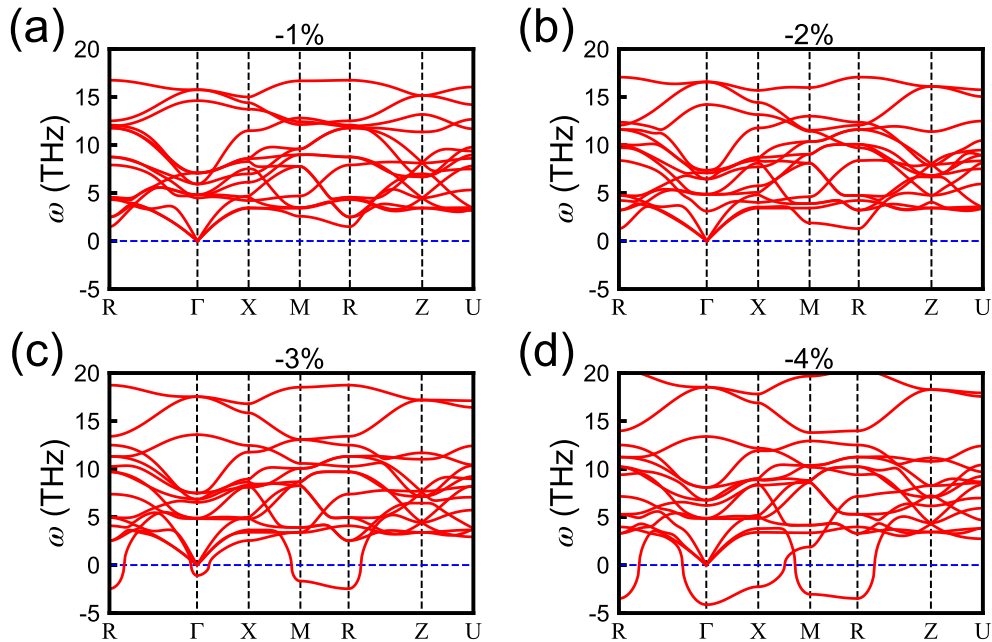


FIG. 2. Phonon band structure of SrCoO₃ under different compressive strains. (a): 1% compressive strain. (b): 2% compressive strain. (c): 3% compressive strain. (d): 4% compressive strain. The coordinates of the high-symmetry \mathbf{k} -points are: $R(0.5, 0.5, 0.5)$, $\Gamma(0.0, 0.0, 0.0)$, $X(0.5, 0.0, 0.0)$, $M(0.5, 0.5, 0.0)$, $Z(0.0, 0.0, 0.5)$, $U(0.5, 0.0, 0.5)$.

To find the most stable crystal structure of SrCoO₃ that arises from the above imaginary phonon modes, we study 4% compressive strain and introduce each imaginary phonon mode as well as their combinations into the simple tetragonal structure (a similar analysis is done on 3% compressive strain and see Supplemental Material [43] Note 4). Since the

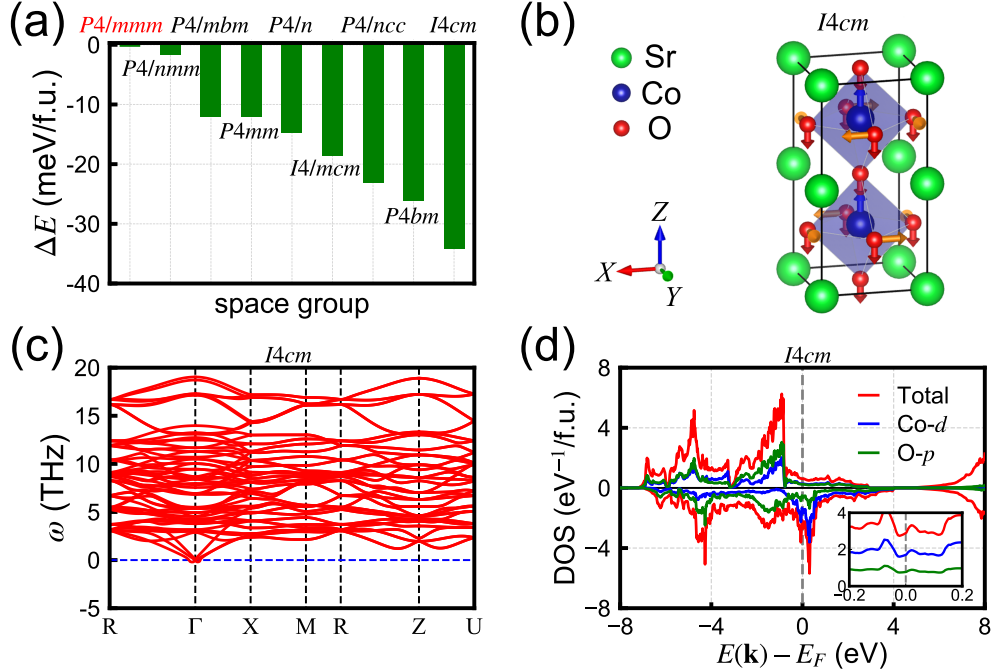


FIG. 3. (a): Total energy of different crystal structures of SrCoO_3 under 4% compressive strain, using the simple tetragonal structure $P4/mmm$ as the zero point. (b): The crystal structure of $I4cm$ SrCoO_3 . The arrows show that the structure has both polar displacements along the c -axis and an out-of-phase oxygen octahedral rotation about the c -axis. (c): Phonon band structure of $I4cm$ SrCoO_3 . (d): Density of states (DOS) of $I4cm$ SrCoO_3 . The red, blue and green curves are total, Co- d projected and O- p projected DOS. Inset: near-Fermi-level DOS (spin up + spin down) of $I4cm$ SrCoO_3 .

imaginary phonons at X and Y points are degenerate, we combine them together and consider it as a “composite” phonon, referred to as X/Y . Thus we have 4 imaginary phonons at Γ , X/Y , M and R . Their combinations (including one phonon mode) yield altogether $C_4^1 + C_4^2 + C_4^3 + C_4^4 = 15$ different cases. However, from our calculations, we find some imaginary phonon modes suppress each other, i.e. when two such imaginary phonons are combined and introduced into the high-symmetry structure, after structural relaxation we end up with a low-symmetry structure that is identical to the one that is derived only from one imaginary phonon. Specifically, we find that the imaginary phonon at R point suppress the imaginary phonon at M point, and the imaginary phonon at Γ -point suppresses the imaginary phonon at X/Y -point. Excluding those cases, we finally end up with 8 low-symmetry structures by introducing the imaginary phonons and their combinations. We

explicitly list below all the 8 low-symmetry structures as well as the associated imaginary phonons:

1. The first low-symmetry structure is obtained by introducing the Γ -point imaginary phonon mode. It is a polar structure. The corresponding space group is $P4mm$ (no. 99) and Glazer notation is $a^0a^0c^0$.
2. The second low-symmetry structure is obtained by introducing the M -point imaginary phonon mode. It is a centrosymmetric structure with an in-phase rotation of CoO_6 oxygen octahedra about the c -axis. The corresponding space group is $P4/mbm$ (no. 127) and Glazer notation $a^0a^0c^+$.
3. The third low-symmetry structure is obtained by introducing the R -point imaginary phonon mode. It is a centrosymmetric structure with an out-of-phase rotation of CoO_6 oxygen octahedra about the c -axis. The corresponding space group is $I4/mcm$ (no. 140) and Glazer notation $a^0a^0c^-$.
4. The fourth low-symmetry structure is obtained by introducing X/Y -point imaginary phonon modes into the simple tetragonal structures. It is an anti-polar structure. The corresponding space group is $P4/nmm$ (no. 129) and Glazer notation is $a^0a^0c^0$.
5. The fifth low-symmetry structure is obtained by introducing M -point and X/Y -point imaginary phonon modes. It is a complicated anti-polar structure with an in-phase rotation of CoO_6 oxygen octahedra about the c -axis. The corresponding space group is $P4/n$ (no. 85) and Glazer notation is $a^0a^0c^+$.
6. The sixth low-symmetry structure is obtained by introducing R -point and X/Y -point imaginary phonon modes. It is a complicated anti-polar structure with an out-of-phase rotation of CoO_6 oxygen octahedra about the c -axis. The corresponding space group is $P4/ncc$ (no. 130) and Glazer notation is $a^0a^0c^-$.
7. The seventh low-symmetry structure is obtained by introducing Γ -point and M -point imaginary phonon modes. It is a polar structure with an in-phase rotation about the c -axis. The corresponding space group is $P4bm$ (no. 100) and Glazer notation $a^0a^0c^+$.

8. The last low-symmetry structure is obtained by introducing Γ -point and R -point imaginary phonon modes. It is a polar structure with an out-of-phase rotation about the c -axis. The corresponding space group is $I4cm$ (no. 108) and Glazer notation $a^0a^0c^-$.

Fig. 3(a) shows the total energy of those new crystal structures (using the simple tetragonal structure $P4/mmm$ as the zero point). We find that the crystal structure of the lowest total energy is the complicated polar structure $I4cm$, which is explicitly shown in Fig. 3(b). To further check that the $I4cm$ structure is indeed dynamically stable, we perform a phonon calculation on the $I4cm$ structure and find no imaginary modes in the phonon spectrum of $I4cm$ SrCoO₃, as shown in Fig. 3(c). In Fig. 3(d), we show the DOS of $I4cm$ SrCoO₃. There is a clear exchange splitting and a finite DOS at the Fermi level. Combining the electronic, magnetic and structural properties shown in Fig. 3, we find that under 4% compressive strain, a ferromagnetic polar metallic state is stabilized in $I4cm$ SrCoO₃. In addition, as we show below, there is a finite range of compressive strain in which SrCoO₃ exhibits a ferromagnetic polar metallic state.

C. Tensile strain

After studying SrCoO₃ under compressive strain, now we switch to tensile strain. We also find a ferromagnetic polar metallic state in SrCoO₃ when the applied tensile strain is appropriate. However, there are some important differences in the nature of polarity.

Similar to compressive strain, SrCoO₃ under tensile strain also naturally transforms to a simple tetragonal structure but with $c/a < 1$. We calculate the phonon spectrum of SrCoO₃ in the simple tetragonal structure under various tensile strains. The results are shown in Fig. 4. We find that under 1% and 2% tensile strains, the phonon spectrum of SrCoO₃ is free from imaginary phonon modes. However, under 3% and 4% tensile strains, imaginary phonon modes appear at Γ and X points. By analyzing the vibration modes, we find that the imaginary phonons at Γ point are two-fold degenerate. They are both polar modes that are associated with the “polarization” of Co and O atoms along a and b axes, respectively. The imaginary phonon at X point is an anti-polar mode with Co and O atoms forming an “out-of-phase local polarization” that points parallel to b -axis and alternates its direction unit cell by unit cell along a axis. We note that due to the C_4 rotation symmetry of the simple tetragonal structure, Y point is equivalent to X point in the Brillouin zone and there

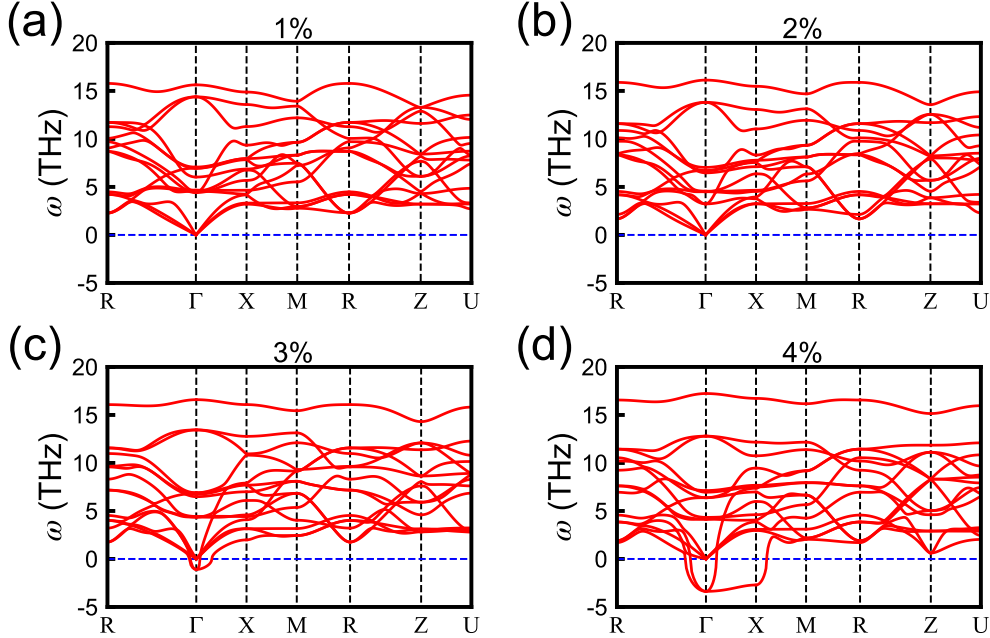


FIG. 4. Phonon band structure of SrCoO_3 under different tensile strains. (a): 1% tensile strain. (b): 2% tensile strain. (c): 3% tensile strain. (d): 4% tensile strain. The coordinates of the high-symmetry \mathbf{k} -points are: $R(0.5, 0.5, 0.5)$, $\Gamma(0.0, 0.0, 0.0)$, $X(0.5, 0.0, 0.0)$, $M(0.5, 0.5, 0.0)$, $Z(0.0, 0.0, 0.5)$, $U(0.5, 0.0, 0.5)$.

is another imaginary anti-polar mode at Y point with Co and O atoms forming an “out-of-phase local polarization” that points parallel to a -axis and alternates its direction unit cell by unit cell along b axis.

Then we study 4% tensile strain and introduce each imaginary phonon mode and their combinations into the simple tetragonal structure (a similar analysis is done on 3% tensile strain and see Supplemental Material [43] Note 4). Again since the imaginary phonons at X and Y points are degenerate, we combine them together and consider it as a “composite” phonon, referred to as X/Y . Similar to the case of 4% compressive strain, we find that the phonon vibration mode at Γ point suppresses the phonon vibration mode at X/Y -point. Therefore, altogether we find two new structures whose energy is lower than that of the simple tetragonal structure.

1. One is a polar structure with no oxygen octahedral rotations, by introducing the Γ -point polar mode into the simple tetragonal structure. The corresponding space group is $Amm2$ (no. 38) and Glazer notation is $a^0a^0c^0$.

2. The other is an anti-polar structure with no oxygen octahedral rotations either, by introducing both X -point and Y -point anti-polar modes into the simple tetragonal structures. The corresponding space group is $P4/mbm$ (no. 127) and Glazer notation is $a^0a^0c^0$.

Fig. 5(a) shows the total energy of these two new crystal structures, using the simple tetragonal $P4/mmm$ as the zero point. We find that the $Amm2$ structure has the lowest total energy. Fig. 5(b) explicitly shows the $Amm2$ structure in which the “polarization” lies along the diagonal line of ab plane. We also test whether this new $Amm2$ structure is dynamically stable. Fig. 5(c) shows the phonon spectrum of $Amm2$ SrCoO_3 and we find no imaginary phonon modes. Fig. 5(d) shows the DOS of $Amm2$ SrCoO_3 , which has a clear exchange splitting and a finite value at the Fermi level. Similar to $I4cm$ SrCoO_3 under 4% compressive strain, combining the electronic, magnetic and structural properties shown in Fig. 5, we find that under 4% tensile strain, a ferromagnetic polar metallic state is also stabilized in $Amm2$ SrCoO_3 . As we show below, there is also a finite range of tensile strain in which SrCoO_3 exhibits a ferromagnetic polar metallic state.

D. Magnetic transition

In the preceding calculations, we assume that SrCoO_3 is in a ferromagnetic metallic state. Previous studies have shown that under biaxial strain, SrCoO_3 exhibits a ferromagnetic-to-antiferromagnetic transition as well as a metal-insulator transition [49, 51, 52]. Following Ref. [51], we consider three common types of antiferromagnetic ordering: A -type with an ordering wave vector $(0, 0, \pi)$, C -type with an ordering wave vector $(\pi, \pi, 0)$ and G -type with an ordering wave vector (π, π, π) . For all these magnetic orderings, we consider various structural distortions with different orientations of “polarization” and different types of oxygen octahedral rotations. After atomic relaxation, for each type of magnetic ordering under a given epitaxial strain, we obtain the most stable crystal structure. Then we compare the total energies of those crystal structures with different types of magnetic ordering. For all the strains considered in this study, we find that SrCoO_3 remains metallic. We show the results in Fig. 6(a). We find that no matter whether SrCoO_3 is in a ferromagnetic state or in an antiferromagnetic state, its most stable structure undergoes a series of distortions and changes in crystal symmetry with an applied biaxial strain. More importantly, within

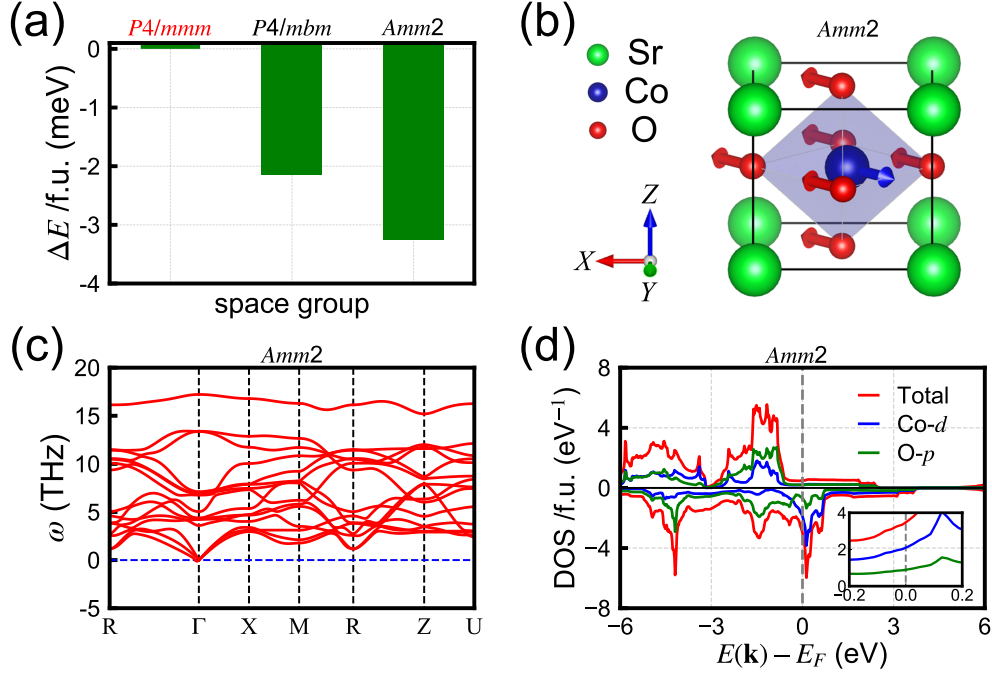


FIG. 5. (a): Total energy of different crystal structures of SrCoO₃ under 4% tensile strain, using the simple tetragonal structure $P4/mmm$ as the zero point. (b): The crystal structure of $Amm2$ SrCoO₃. The arrows show that the structure has polar displacements along the diagonal line in the ab plane. (c): Phonon band structure of $Amm2$ SrCoO₃. (d): Density of states (DOS) of $Amm2$ SrCoO₃. The red, blue and green curves are total, Co- d projected and O- p projected DOS. Inset: near-Fermi-level DOS (spin up + spin down) of $Amm2$ SrCoO₃.

4% compressive or tensile strain, the ferromagnetic ordering always has lower energy than the antiferromagnetic orderings. Fig. 6(b) summarizes the phase diagram of SrCoO₃ as a function of epitaxial biaxial strain. Under a compressive strain from 2.4% to 4%, SrCoO₃ is in a ferromagnetic polar metallic state with “polarization” along the c -axis (dark red range). Under a tensile strain from 2.9% to 4%, SrCoO₃ is also in a ferromagnetic polar metallic state with “polarization” lying in the ab -plane (light red range). In between, SrCoO₃ is a ferromagnetic metal with inversion symmetry. Finally, we note that if the applied strain is larger than 4%, a ferromagnetic-to-antiferromagnetic transition may occur to SrCoO₃ (see Supplemental Material [43] Note 5 for details).

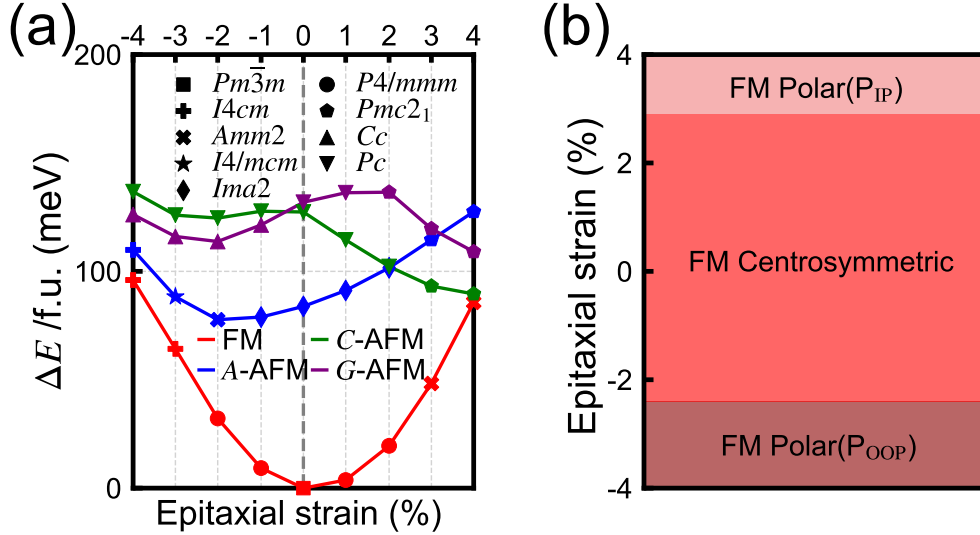


FIG. 6. (a): An energy diagram of SrCoO_3 as a function of epitaxial strain. Red, blue, green and purple colors represent ferromagnetic order (FM), A -type antiferromagnetic order (A -AFM), C -type antiferromagnetic order (C -AFM) and G -type antiferromagnetic order (G -AFM). Different symbols represent different crystal structure symmetries (the space group is shown). The energy of cubic FM SrCoO_3 is used as the zero point. (b): A phase diagram of SrCoO_3 as a function of epitaxial strain. “ P_{IP} ” means “polarization” lying in the ab -plane and “ P_{OOP} ” means “polarization” pointing along the c -axis.

IV. CONCLUSION

In summary, via first-principles calculations, we show that epitaxial strain engineering provides a simple alternative to synthesizing new materials in the search for magnetic polar metals. We demonstrate this route in a ferromagnetic metallic oxide SrCoO_3 . We find that using either a compressive or tensile strain of experimentally feasible magnitude can induce a ferromagnetic polar metallic state in SrCoO_3 . Specifically, under a compressive strain of 2.4%-4%, an $I4cm$ structure is stabilized in SrCoO_3 with the “polarization” pointing along the c -axis as well as an out-of-phase oxygen octahedral rotation about the c -axis. Under a tensile strain of 2.9%-4%, an $Amm2$ structure is stabilized in SrCoO_3 with the “polarization” lying in the ab -plane but with no oxygen octahedral rotations. In addition, we find that under sufficiently large epitaxial strain ($> 4\%$), a ferromagnetic-to-antiferromagnetic transition may occur to SrCoO_3 . Such a large strain is challenging via epitaxy but might be achieved

in freestanding thin films [53]. We hope that our work may stimulate further theory and experiment studies on the search for magnetic polar metals.

ACKNOWLEDGMENTS

We are grateful to Pu Yu for useful discussions. This project was financially supported by the National Key R&D Program of China under project number 2021YFE0107900, the National Natural Science Foundation of China under project number 12374064, Science and Technology Commission of Shanghai Municipality under grant number 23ZR1445400 and a grant from the New York University Research Catalyst Prize. NYU High-Performance-Computing (HPC) provides computational resources.

-
- [1] R. E. Cohen, Origin of ferroelectricity in perovskite oxides, *Nature* **358**, 136 (1992).
- [2] T. Goto, T. Kimura, G. Lawes, A. P. Ramirez, and Y. Tokura, Ferroelectricity and Giant Magnetocapacitance in Perovskite Rare-Earth Manganites, *Phys. Rev. Lett.* **92**, 257201 (2004).
- [3] I. Inbar and R. E. Cohen, Comparison of the electronic structures and energetics of ferroelectric LiNbO_3 and LiTaO_3 , *Phys. Rev. B* **53**, 1193 (1996).
- [4] M. B. Smith, K. Page, T. Siegrist, P. L. Redmond, E. C. Walter, R. Seshadri, L. E. Brus, and M. L. Steigerwald, Crystal Structure and the Paraelectric-to-Ferroelectric Phase Transition of Nanoscale BaTiO_3 , *J. Am. Chem. Soc.* **130**, 6955 (2008).
- [5] J. Wang, J. B. Neaton, H. Zheng, V. Nagarajan, S. B. Ogale, B. Liu, D. Viehland, V. Vaithyanathan, D. G. Schlom, U. V. Waghmare, et al., Epitaxial BiFeO_3 Multiferroic Thin Film Heterostructures, *Science* **299**, 1719 (2003).
- [6] S.-W. Cheong and M. Mostovoy, Multiferroics: a magnetic twist for ferroelectricity, *Nat. Mater.* **6**, 13 (2007).
- [7] R. Ramesh and N. A. Spaldin, Multiferroics: progress and prospects in thin films, *Nat. Mater.* **6**, 21 (2007).
- [8] H. Zheng, J. Wang, S. E. Lofland, Z. Ma, L. Mohaddes-Ardabili, T. Zhao, L. Salamanca-Riba, S. R. Shinde, S. B. Ogale, F. Bai, et al., Multiferroic $\text{BaTiO}_3\text{-CoFe}_2\text{O}_4$ Nanostructures, *Science* **303**, 661 (2004).
- [9] B. Neese, B. Chu, S.-G. Lu, Y. Wang, E. Furman, and Q. M. Zhang, Large Electrocaloric Effect in Ferroelectric Polymers Near Room Temperature, *Science* **321**, 821 (2008).
- [10] P. W. Anderson and E. I. Blount, Symmetry Considerations on Martensitic Transformations: "Ferroelectric" Metals?, *Phys. Rev. Lett.* **14**, 217 (1965).
- [11] Y. Shi, Y. Guo, X. Wang, A. J. Princep, D. Khalyavin, P. Manuel, Y. Michiue, A. Sato, K. Tsuda, S. Yu, et al., A ferroelectric-like structural transition in a metal, *Nat. Mater.* **12**, 1024 (2013).
- [12] S. Lei, M. Gu, D. Puggioni, G. Stone, J. Peng, J. Ge, Y. Wang, B. Wang, Y. Yuan, K. Wang, et al., Observation of Quasi-Two-Dimensional Polar Domains and Ferroelastic Switching in a Metal, $\text{Ca}_3\text{Ru}_2\text{O}_7$, *Nano Lett.* **18**, 3088 (2018).

- [13] T. H. Kim, D. Puggioni, Y. Yuan, L. Xie, H. Zhou, N. Campbell, P. J. Ryan, Y. Choi, J.-W. Kim, J. R. Patzner, et al., Polar metals by geometric design, *Nature* **533**, 68 (2016).
- [14] K. S. Takahashi, Y. Matsubara, M. S. Bahramy, N. Ogawa, D. Hashizume, Y. Tokura, and M. Kawasaki, Polar metal phase stabilized in strained La-doped BaTiO₃ films, *Sci. Rep.* **7**, 4631 (2017).
- [15] Y.-W. Fang and H. Chen, Design of a multifunctional polar metal via first-principles high-throughput structure screening, *Commun. Mater.* **1**, 1 (2020).
- [16] E. I. P. Aulestia, Y. W. Cheung, Y.-W. Fang, J. He, K. Yamaura, K. T. Lai, S. K. Goh, and H. Chen, Pressure-induced enhancement of non-polar to polar transition temperature in metallic LiOsO₃, *Appl. Phys. Lett.* **113** (2018).
- [17] C. Xia, Y. Chen, and H. Chen, Coexistence of polar displacements and conduction in doped ferroelectrics: An ab initio comparative study, *Phys. Rev. Mater.* **3**, 054405 (2019).
- [18] C. Enderlein, J. F. de Oliveira, D. A. Tompsett, E. B. Saitovitch, S. S. Saxena, G. G. Lonzarich, and S. E. Rowley, Superconductivity mediated by polar modes in ferroelectric metals, *Nat. Commun.* **11**, 4852 (2020).
- [19] D. Puggioni, G. Giovannetti, and J. M. Rondinelli, Polar metals as electrodes to suppress the critical-thickness limit in ferroelectric nanocapacitors, *J. Appl. Phys.* **124** (2018).
- [20] Y. Jiao, Y.-W. Fang, J. Sun, P. Shan, Z. Yu, H. L. Feng, B. Wang, H. Ma, Y. Uwatoko, K. Yamaura, et al., Coupled magnetic and structural phase transitions in the antiferromagnetic polar metal Pb₂CoOsO₆ under pressure, *Phys. Rev. B* **102**, 144418 (2020).
- [21] S. Lei, S. Chikara, D. Puggioni, J. Peng, M. Zhu, M. Gu, W. Zhao, Y. Wang, Y. Yuan, H. Akamatsu, et al., Comprehensive magnetic phase diagrams of the polar metal Ca₃(Ru_{0.95}Fe_{0.05})₂O₇, *Phys. Rev. B* **99**, 224411 (2019).
- [22] M. Meng, Z. Wang, A. Fathima, S. Ghosh, M. Saghayezhian, J. Taylor, R. Jin, Y. Zhu, S. T. Pantelides, J. Zhang, et al., Interface-induced magnetic polar metal phase in complex oxides, *Nat. Commun.* **10**, 5248 (2019).
- [23] H. Zhang, Y.-T. Shao, R. Chen, X. Chen, S. Susarla, D. Raftrey, J. T. Reichanadter, L. Caretta, X. Huang, N. S. Settineri, et al., A room temperature polar magnetic metal, *Phys. Rev. Mater.* **6**, 044403 (2022).
- [24] H. Zhang, D. Raftrey, Y.-T. Chan, Y.-T. Shao, R. Chen, X. Chen, X. Huang, J. T. Reichanadter, K. Dong, S. Susarla, et al., Room-temperature skyrmion lattice in a layered mag-

- net $(\text{Fe}_{0.5}\text{Co}_{0.5})_5\text{GeTe}_2$, *Sci. Adv.* **8**, eabm7103 (2022).
- [25] D. Tian, Z. Liu, S. Shen, Z. Li, Y. Zhou, H. Liu, H. Chen, and P. Yu, Manipulating Berry curvature of SrRuO_3 thin films via epitaxial strain, *Proc. Natl. Acad. Sci.* **118** (2021).
- [26] D. G. Schlom, L.-Q. Chen, C.-B. Eom, K. M. Rabe, S. K. Streiffer, and J.-M. Triscone, Strain Tuning of Ferroelectric Thin Films, *Annu. Rev. Mater. Res.* **37**, 589 (2007).
- [27] J. H. Lee, L. Fang, E. Vlahos, X. Ke, Y. W. Jung, L. F. Kourkoutis, J.-W. Kim, P. J. Ryan, T. Heeg, M. Roeckerath, et al., A strong ferroelectric ferromagnet created by means of spin–lattice coupling, *Nature* **466**, 954 (2010).
- [28] C. J. Fennie and K. M. Rabe, Magnetic and Electric Phase Control in Epitaxial EuTiO_3 from First Principles, *Phys. Rev. Lett.* **97**, 267602 (2006).
- [29] J. H. Lee and K. M. Rabe, Epitaxial-Strain-Induced Multiferroicity in SrMnO_3 from First Principles, *Phys. Rev. Lett.* **104**, 207204 (2010).
- [30] J. H. Haeni, P. Irvin, W. Chang, R. Uecker, P. Reiche, Y. L. Li, S. Choudhury, W. Tian, M. E. Hawley, B. Craigo, et al., Room-temperature ferroelectricity in strained SrTiO_3 , *Nature* **430**, 758 (2004).
- [31] R. J. Zeches, M. D. Rossell, J. X. Zhang, A. J. Hatt, Q. He, C.-H. Yang, A. Kumar, C. H. Wang, A. Melville, C. Adamo, et al., A Strain-Driven Morphotropic Phase Boundary in BiFeO_3 , *Science* **326**, 977 (2009).
- [32] R. H. Potze, G. A. Sawatzky, and M. Abbate, Possibility for an intermediate-spin ground state in the charge-transfer material SrCoO_3 , *Phys. Rev. B* **51**, 11501 (1995).
- [33] Y. Long, Y. Kaneko, S. Ishiwata, Y. Taguchi, and Y. Tokura, Synthesis of cubic SrCoO_3 single crystal and its anisotropic magnetic and transport properties, *J Phys: condens. Mat.* **23**, 245601 (2011).
- [34] P. Hohenberg and W. Kohn, Inhomogeneous Electron Gas, *Phys. Rev.* **136**, B864 (1964).
- [35] W. Kohn and L. J. Sham, Self-Consistent Equations Including Exchange and Correlation Effects, *Phys. Rev.* **140**, A1133 (1965).
- [36] G. Kresse and J. Hafner, *Ab initio* molecular-dynamics simulation of the liquid-metal–amorphous-semiconductor transition in germanium, *Phys. Rev. B* **49**, 14251 (1994).
- [37] G. Kresse and J. Furthmüller, Efficient iterative schemes for *ab initio* total-energy calculations using a plane-wave basis set, *Phys. Rev. B* **54**, 11169 (1996).

- [38] J. P. Perdew, K. Burke, and M. Ernzerhof, Generalized Gradient Approximation Made Simple, *Phys. Rev. Lett.* **77**, 3865 (1996).
- [39] H. J. Monkhorst and J. D. Pack, Special points for Brillouin-zone integrations, *Phys. Rev. B* **13**, 5188 (1976).
- [40] G. Kresse, J. Furthmüller, and J. Hafner, *Ab initio* Force Constant Approach to Phonon Dispersion Relations of Diamond and Graphite, *Europhys. Lett.* **32**, 729 (1995).
- [41] K. Parlinski, Z. Q. Li, and Y. Kawazoe, First-Principles Determination of the Soft Mode in Cubic ZrO₂, *Phys. Rev. Lett.* **78**, 4063 (1997).
- [42] A. Togo and I. Tanaka, First principles phonon calculations in materials science, *Scripta. Mater.* **108**, 1 (2015).
- [43] See Supplemental Material at xxx for the discussion on Hubbard U , additional structural and phonon properties of SrCoO₃, as well as further discussion on antiferromagnetic ordering, which also includes Ref. [44].
- [44] G. Gou, I. Grinberg, A. M. Rappe, and J. M. Rondinelli, Lattice normal modes and electronic properties of the correlated metal LaNiO₃, *Phys. Rev. B* **84**, 144101 (2011).
- [45] H. T. Stokes, E. H. Kisi, D. M. Hatch, and C. J. Howard, Group-theoretical analysis of octahedral tilting in ferroelectric perovskites, *Acta. Crystallogr. Sect. B: Struct. Sci.* **58**, 934 (2002).
- [46] P. Bezdzicka, A. Wattiaux, J. C. Grenier, M. Pouchard, and P. Hagenmuller, Preparation and characterization of Fully stoichiometric SrCoO₃ by electrochemical oxidation, *Z. Anorg. Allg. Chem.* **619**, 7 (1993).
- [47] M. Zhuang, W. Zhang, A. Hu, and N. Ming, Possible magnetic ground state in the perovskite SrCoO₃, *Phys. Rev. B* **57**, 13655 (1998).
- [48] P. Ravindran, P. A. Korzhavyi, H. Fjellvåg, and A. Kjekshus, Electronic structure, phase stability, and magnetic properties of La_{1-x}Sr_xCoO₃ from first-principles full-potential calculations, *Phys. Rev. B* **60**, 16423 (1999).
- [49] Y. Wang, Q. He, W. Ming, M.-H. Du, N. Lu, C. Cafolla, J. Fujioka, Q. Zhang, D. Zhang, S. Shen, et al., Robust Ferromagnetism in Highly Strained SrCoO₃ Thin Films, *Phys. Rev. X* **10**, 021030 (2020).
- [50] I. Pallikara, P. Kayastha, J. M. Skelton, and L. D. Whalley, The physical significance of imaginary phonon modes in crystals, *Electron. Struct.* **4**, 033002 (2022).

- [51] J. H. Lee and K. M. Rabe, Coupled Magnetic-Ferroelectric Metal-Insulator Transition in Epitaxially Strained SrCoO₃ from First Principles, *Phys. Rev. Lett.* **107**, 067601 (2011).
- [52] S. J. Callori, S. Hu, J. Bertinshaw, Z. J. Yue, S. Danilkin, X. L. Wang, V. Nagarajan, F. Klose, J. Seidel, and C. Ulrich, Strain-induced magnetic phase transition in SrCoO_{3- δ} thin films, *Phys. Rev. B* **91**, 140405 (2015).
- [53] S. S. Hong, M. Gu, M. Verma, V. Harbola, B. Y. Wang, D. Lu, A. Vailionis, Y. Hikita, R. Pentcheva, J. M. Rondinelli, et al., Extreme tensile strain states in La_{0.7}Ca_{0.3}MnO₃ membranes, *Science* **368**, 71 (2020).